THE UNIVERSITY OF MICHIGAN
COLLEGE OF ENGINEERING
Department of Atmospheric and Oceanic Science

Technical Report

RESEARCH NOTES

Aksel C. Wiin-Nielsen
Project Director

DRDA Project 002630

supported by:

NATIONAL SCIENCE FOUNDATION
GRANT NO. GA-16166
WASHINGTON, D.C.

administered through:

DIVISION OF RESEARCH DEVELOPMENT AND ADMINISTRATION ANN ARBOR

May 1974

TABLE OF CONTENTS

A NOTE ON THE MOTION OF INERTIAL WAVES ON THE SPHERE

by

A. Wiin-Nielsen
Department of Atmospheric and Oceanic Science
The University of Michigan

Abstract

The motion of inertial waves on the spherical earth is found as a function of the zonal wave number by using a perturbation method with a basic state of no motion. The speed of the waves is compared with the elementary wave formula, derived under the assumption of a constant Coriolis parameter. The inertial waves can be investigated as a special case of a more general investigation, conducted earlier by the author, of transient waves in the atmosphere.

1. Introduction

The motion of inertial waves is generally described by the well-known formula $\pm f_o/k$ where f_o is a constant value of the Coriolis parameter while k is the wave number. It is obvious that the formula is valid formally for short waves only because no variation of the Coriolis parameter is permitted. Inertial trajectories on the spherical earth have recently been investigated by Wiin-Nielsen (1973) showing marked deviations from the inertial circle for large initial wind speeds and/or initial positions in the very low latitudes. It would appear worthwhile to investigate if corresponding differences are found between the simple wave formula given above and speeds computed without the simplifying assumptions.

The author (Wiin-Nielsen, 1971) has investigated the general problem of the motion of the vertical modes of transient waves in an atmospheric basic state characterized by no motion, but an arbitrary thermal stratification. It was found that the speed of the waves is determined by three coupled, ordinary differential equations involving the streamfunction, the velocity potential and the geopotential for a given vertical mode of the perturbation. The inertial waves are characterized as the waves which would exist if there were no pressure field. It follows therefore that we may obtain the equations governing the motion of inertial waves by simply disregarding all reference to the geopotential of the perturbation. In this way we obtain two coupled equations which can be solved by using a numerical technique analogous to the one employed in the earlier investigation.

2. Problem and Procedures

The perturbation equations for inertial waves on a basic state of no motion are

$$\frac{\partial u}{\partial t} = fv$$

$$\frac{\partial v}{\partial t} = -fu \qquad (2.1)$$

where $f = 2\Omega \sin \varphi$. (u,v) is the horizontal velocity vector, u the zonal velocity, v the meridional velocity, t time, Ω the angular velocity of the earth, and φ latitude.

The system (2.1) is replaced by the vorticity and the divergence equations:

$$\frac{\partial \zeta}{\partial t} = -f\nabla \cdot \vec{v} - \frac{2\Omega}{a} \cos\varphi \cdot v$$

$$\frac{\partial \nabla \cdot \vec{v}}{\partial t} = f\zeta - \frac{2\Omega}{a} \cos\varphi \cdot u \tag{2.2}$$

where $\zeta = \nabla^2\psi$, $\nabla \cdot \vec{v} = \nabla^2\chi$ and

$$\nabla^2 = \frac{1}{a^2}\nabla_s^2 = \frac{1}{a^2}\left[\frac{1}{\cos^2\varphi}\frac{\partial^2}{\partial\lambda^2} + \frac{1}{\cos\varphi}\frac{\partial}{\partial\varphi}\left(\cos\varphi\frac{\partial}{\partial\varphi}\right)\right] \tag{2.3}$$

in which a is the radius of the earth, λ the longitude, ζ the vorticity, $\nabla \cdot \vec{v}$ the divergence, ψ the streamfunction, and χ the velocity potential. Note, that

$$u = -\frac{1}{a}\frac{\partial\psi}{\partial\varphi} + \frac{1}{a\cos\varphi}\frac{\partial\chi}{\partial\lambda}$$

$$v = \frac{1}{a\cos\varphi}\frac{\partial\psi}{\partial\lambda} + \frac{1}{a}\frac{\partial\chi}{\partial\varphi} \tag{2.4}$$

We notice that all the dependent variables can be expressed in terms of the streamfunction and the velocity potential. The perturbations are expressed in the form

$$\psi = \psi_m(\varphi)\, e^{im(\lambda - ct)}$$

$$\chi = i\chi_m(\varphi)\, e^{im(\lambda - ct)} \tag{2.5}$$

Introducing the nondimensional phase speed s by the relation

$$s = -\frac{\nu}{2\Omega} = -\frac{mc}{2\Omega} \tag{2.6}$$

where ν is the frequency, we find after substitution of (2.5) in (2.2) that

$$s \nabla_s^2 \psi_m + m\psi_m + (1-\mu^2) \frac{\partial \chi_m}{\partial \mu} + \mu \nabla_s^2 \chi_m = 0$$

$$s \nabla_s^2 \chi_m + m\chi_m + (1-\mu^2) \frac{\partial \psi_m}{\partial \mu} + \mu \nabla_s^2 \psi_m = 0 \qquad (2.7)$$

in which $\mu = \sin \varphi$.

The problem is now to solve the eigenvalue problem presented by (2.7) in which s is the eigenvalue. We obtain a numerical procedure to find the desired eigenvalues by expanding ψ_m and χ_m in series of Legendre functions, i.e.,

$$a_m(\mu) = \sum_{r=0}^{R} \hat{a}(m, m+2r)\, P(m, m+2r, \mu)$$

or

$$a_m(\mu) = \sum_{r=0}^{R} \hat{a}(m, m+2r+1)\, P(m, m+2r+1, \mu) \qquad (2.8)$$

in which $R = r_{max}$ denotes the truncation in the series (2.8), and where the first and second forms are used for even and odd functions, respectively, (2.8) are substituted in (2.7). Making use of a number of identities for the set of Legendre functions we can reduce the resulting equations to the following pair for each value of r:

$$-\frac{(2r+1)(m+2r)}{(m+2r+1)(m+4r+1)} \hat{\chi}(m, m+2r)$$

$$+\left\{\frac{m}{(m+2r+1)(m+2r+2)} - s\right\} \hat{\psi}(m, m+2r+1)$$

$$-\frac{(m+2r+3)(2m+2r+2)}{(m+2r+2)(2m+4r+5)} \hat{\chi}(m, m+2r+2) = 0$$

$$-\frac{2r(m+2r-1)}{(m+2r)(2m+4r-1)} \hat{\psi}(m, m+2r-1)$$

$$+\left\{\frac{m}{(m+2r)(2m+2r-1)} - s\right\} \hat{\chi}(m, m+2r)$$

$$-\frac{(m+2r+2)(2m+2r+1)}{(m+2r+1)(2m+4r+3)} \hat{\psi}(m, m+2r+1) = 0 \qquad (2.9)$$

We notice from (2.9) that even functions for the streamfunction are coupled with odd functions for the velocity potential and vice versa. For a given value of m the parameter r will run through the values 0,1,2,...,R. We

have thus $2(R+1)$ equations which leads to finding the eigenvalues in a standard eigenvalue matrix. It is not obvious at the outset how large R must be in order to determine the largest eigenvalues with sufficient accuracy. This problem was solved experimentally by gradually increasing R in steps of 1 until no change was found in the largest eigenvalues. Experience showed that R in no case needed to exceed 20.

3. Results

The system (2.9) was solved as described above for a fixed value of m, selecting R in such a way that we have a good accuracy for the largest eigenvalues. Using this procedure we can repeat the calculation for a set of values of m and thereby get the phase speed as a function of the zonal wave number. These calculations were carried through for the values m = 1,2,...,15. For each value of m we have determined the first six eigenvalues. As one would expect from the simple theory with a constant Coriolis parameter the eigenvalues appear in pairs with approximately the same absolute value, but of opposite sign. Table I gives the numerical values of c, expressed in the unit: deg day^{-1}, for the first six eigenvalues. The computed values of s were converted to c using (2.6) and a value of Ω = 360 deg day^{-1}. It is seen that c decreases in absolute value as m increases for each of the six eigenvalues.

TABLE I

NUMERICAL VALUES OF THE FIRST SIX EIGENVALUES
(Expressed in the unit: deg day^{-1})

m	c_1	c_2	c_3	c_4	c_5	c_6
1	-720.14	716.76	-714.15	708.27	-703.97	
2	-359.58	357.20	-356.43	352.25	-351.51	345.57
3	-239.05	237.27	-236.44	233.54	-232.69	228.73
4	-178.72	177.27	-176.42	174.17	-173.30	170.31
5	-142.49	141.23	-140.38	138.52	-137.68	135.25
6	-118.30	117.19	-116.35	114.75	-113.92	111.89
7	-101.00	100.00	- 99.16	97.77	- 96.96	95.20
8	- 88.01	87.10	- 86.27	85.03	- 84.23	82.69
9	- 77.89	77.06	- 76.24	75.12	- 74.34	72.97
10	- 69.79	69.02	- 68.22	67.20	- 66.43	65.19
11	- 63.16	62.44	- 61.65	60.71	- 59.97	58.84
12	- 57.63	56.96	- 56.18	55.31	- 54.58	53.55
13	- 52.94	52.31	- 51.54	50.74	- 50.03	49.08
14	- 48.93	48.33	- 47.58	46.83	- 46.13	45.25
15	- 45.45	44.88	- 44.14	43.44	- 42.76	41.94

One of the first problems to investigate is if the values in Table I agree reasonably well with the simple formula $\pm f_o/k$. In order to make such a comparison we write

$$c = \frac{f_o}{k} = \frac{2\Omega \sin \varphi_o}{2\pi} \cdot L = \frac{2\Omega \sin \varphi_o}{2\pi} \cdot \frac{360^\circ}{m} = \frac{720^\circ \sin \varphi_o}{m} \tag{3.1}$$

where we have expressed the wavelength in degrees of longitude and $\Omega = 2\pi$ day^{-1}. It is obvious that if (3.1) shall give values in agreement with the numerical values in Table I we must select $\varphi_o = 1/2\pi$. The solid curve in Figure 1 displays the relation $c = 720/m$, while the circles give the values of c_6 from Table I. It is obvious that the values $|c_1|, |c_2|, \ldots, |c_5|$ would be even closer. We have therefore shown empirically that the phase speed of inertial waves are well approximated by a formula where the phase speed is inversely proportional to the zonal wave number. This relation is of course not exact. If it were, we would, according to (2.6), have $s = 1$ as the eigenvalue. The numerical determination of s shows, however, that the largest eigenvalue s_1 deviate only slightly from unity as shown in Table II.

TABLE II

THE LARGEST EIGENVALUE s_1 AS A FUNCTION OF m

m	1	2	3	4	5	6	7	8
s_1	0.9978	0.9964	0.9936	0.9905	0.9871	0.9834	0.9795	0.9755

9	10	11	12	13	14	15
0.9713	0.9670	0.9626	0.9581	0.9536	0.9490	0.9445

4. Concluding Remarks

The speed of inertial waves on the sphere has been calculated. The results show that the various eigenvalues, ordered according to their absolute value for the same value of the longitudinal wave number, decrease relatively little. It is also shown that the phase speed of the inertial waves is, for practical purposes inversely proportional to the longitudinal wave number.

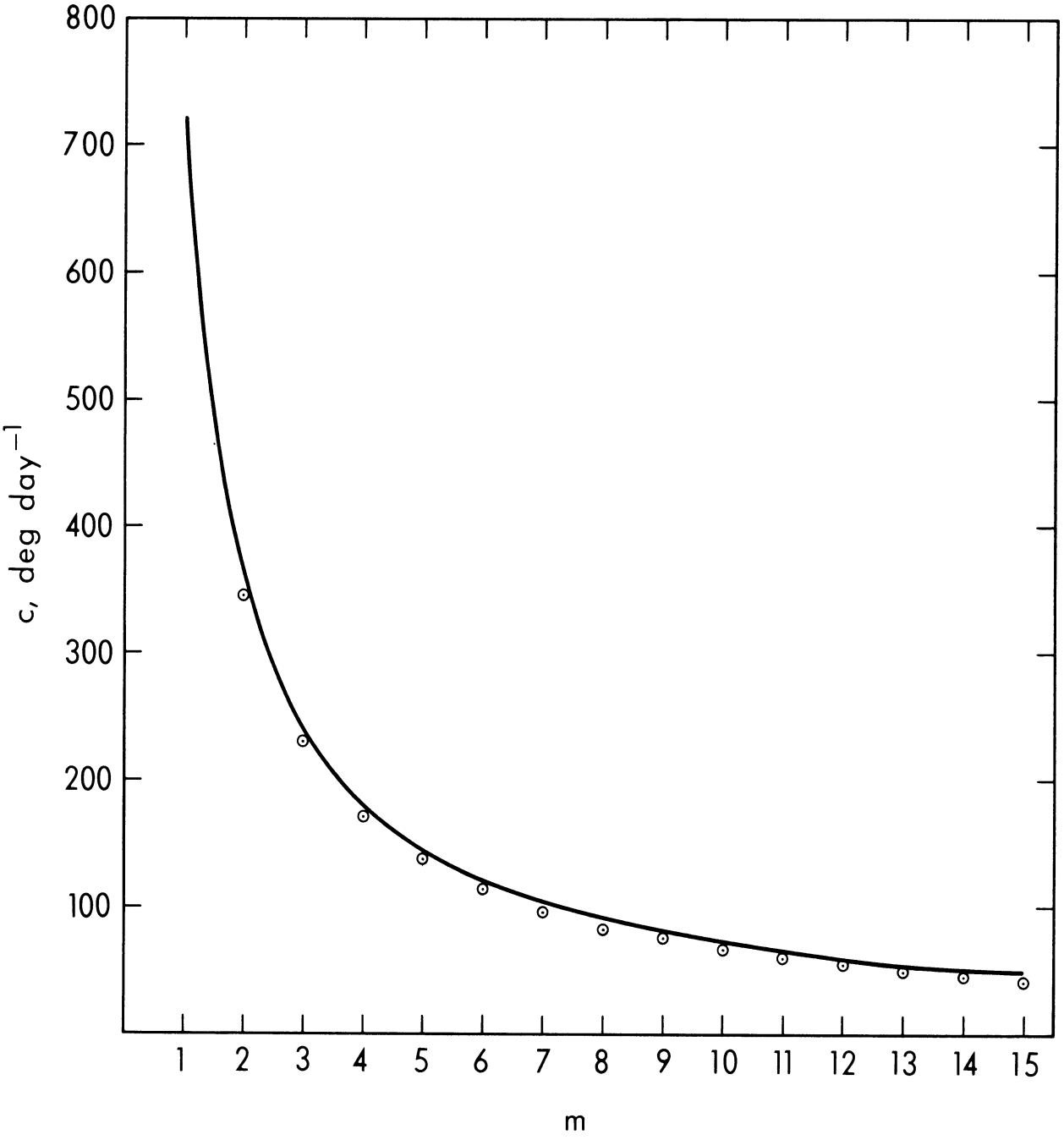

Figure 1. The curve shows the relation c = 720/m while the circles indicate the values c_6 taken from Table I.

It is naturally possible to calculate the functions $\psi_m(\mu)$ and $\chi_m(\mu)$ by summing the series (2.8) after having found the eigenvector $\hat{\psi}(m, m+2r)$ and $\hat{\chi}(m, m+2r)$ from the solution of the system (2.9). Such calculations have been made, but the results are not reproduced here because no significant conclusions have been drawn from the results.

5. Acknowledgment

The research leading to this paper has been supported by the National Science Foundation under Grant No. GA-16166. Mr. James Pfaendtner has been responsible for the programming of the numerical calculations.

References

Wiin-Nielsen, A., 1971: On the motion of various vertical modes of transient, very long waves, Part II, the spherical case, Tellus, Vol. 23, No. 3, pp. 207-217.

Wiin-Nielsen, A., 1973: On the inertial flow on the sphere, Technical Report, The University of Michigan, 002630-6-T, 52 pp.

A NOTE ON BAROCLINIC INSTABILITY AS A FUNCTION OF THE VERTICAL WIND PROFILE

by

A. Wiin-Nielsen
Department of Atomspheric and Oceanic Science
The University of Michigan

Abstract

The note provides an additional example of a solution of the quasi-geostrophic, baroclinic stability problem in an atmosphere with adiabatic stratification. The main purpose of the example is to consider wind profiles in which the maximum may vary in position. For each profile it is possible to determine the region of instability in a diagram with the maximum wind as ordinate and the wavelength as abscissa. In additon, the degree of instability, measured by either the imaginary part of the wave speed or by the e-folding time, can be calculated.

1. Introduction

A few years ago the author gave a solution of the quasi-geostrophic, baroclinic stability problem in an atmosphere with adiabatic, vertical stratification with a arbitrary vertical profile of the horizontal wind in the basic state (Wiin-Nielsen, 1967). Several examples were given in the original paper. The purpose of this note is to provide an additional example using a wind profile which is rather general.

2. Review of the Solution

The eigenvalue problem for the adiabatic, quasi-geostrophic stability question may be stated by the following equation for the (complex) amplitude of the perturbation "vertical velocity" $\Omega = \Omega(p_*)$, where p_* is a nondimensional pressure, $p_* = p/p_o$, p is pressure and $p_o = 100$ cb:

$$E(E - c)\frac{d^2\Omega}{dp_*^2} - (2E - c)\frac{dE}{dp_*}\frac{d\Omega}{dp_*} = 0 \tag{2.1}$$

where $E = U(p_*) - c$, $U = U(p_*)$ the given wind profile, c the (complex) phase speed, $c_r = \beta/k^2$, β the Rossby parameter, k the wave number and where the perturbations are of the form

$$\omega = \Omega(p_*)\exp[ik(x - ct)] \tag{2.2}$$

The solution to (2.1) was given in the previous paper by the expression

$$c = (I_1 - \frac{1}{2}c_R) \pm (I_1^2 - I_2 + \frac{1}{4}c_R^2)^{\frac{1}{2}} \tag{2.3}$$

in which

$$I_1 = \int_o^1 U\,dp_* \tag{2.4}$$

and

$$I_2 = \int_o^1 U^2\,dp_* \tag{2.5}$$

3. A New Example

We shall prescribe the vertical profile of the horizontal wind by the expression

$$U_N(p_*) = \frac{(n-1)!}{(r-1)!(n-r-1)!} p_*^{r-1}(1-p_*)^{n-r-1} \tag{3.1}$$

where $U_N = U/U_m$, U_m is the vertical average of the wind, i.e., $U_m = I_1$, P_* is the nondimensional pressure, while r and n are parameters which determine the shape of the wind profile. It is seen that (3.1) is closely related to the well-known beta function, and that the expression in the first fraction guarantees that

$$\int_0^1 U_N(p_*)\, dp_* = 1 \tag{3.2}$$

Some selected examples of the vertical wind profiles given by (3.1) are shown in Figure 1. It is seen that the parameter n, for a fixed value of r, determines the position of the maximum in such a way that increasing values of n corresponds to a maximum wind at lower values of the pressure. As seen from Figure 1 it is possible to produce many shapes of the wind profile by selecting r and n in a suitable way. For example, n = 2r will produce a wind profile which has its maximum at $p_* = 0.5$ and is symmetric around this level. (r,n) = (2,4) (3,6), (4,8), and (5,10) are examples of such profiles. We note furthermore that if we in (3.1) replace r by $n - r_1$, but keep n the same we get a profile

$$U_N(p_*) = \frac{(n-1)!}{(n-r_1-1)!(r_1-1)!} p_*^{n-r_1-1}(1-p_*)^{r_1-1} \tag{3.3}$$

Introducing for convenience the variable $p_* = s + 1/2$ we find (3.1) to be

$$U_N(s) = \frac{(n-1)!}{(r-1)!(n-r-1)!}\left(\frac{1}{2}+s\right)^{r-1}\left(\frac{1}{2}-s\right)^{n-r-1} \tag{3.4}$$

while (3.2) becomes

$$U_N(s) = \frac{(n-1)!}{(n-r_1-1)!(r_1-1)!}\left(\frac{1}{2}+s\right)^{n-r_1-1}\left(\frac{1}{2}-s\right)^{r_1-1} \tag{3.5}$$

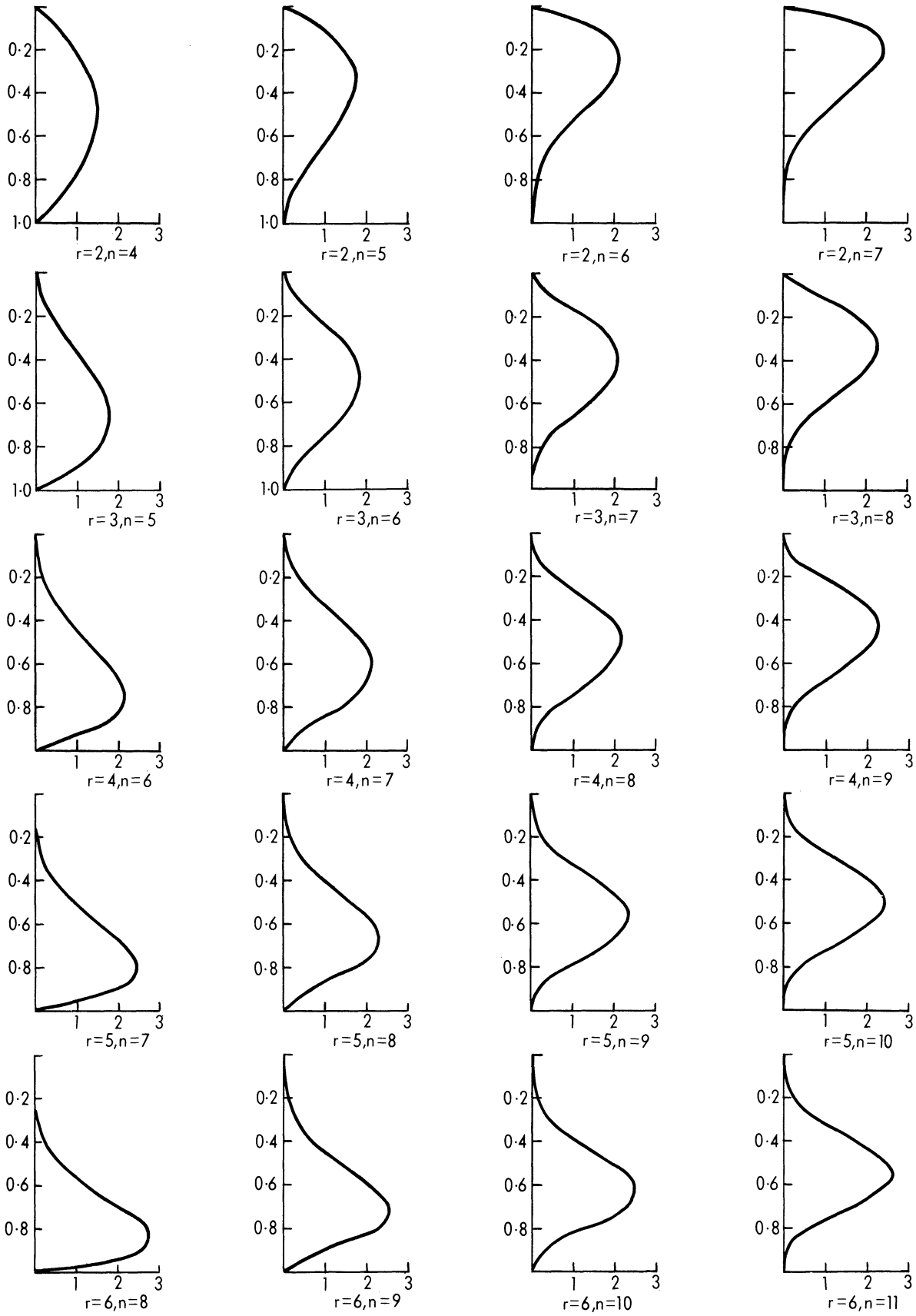

Figure 1. Examples of wind profiles for various values of (r,n). The curves have nondimensional pressure as the ordinate and the nondimensional basic current as abscissa.

The variable s goes from the value -1/2 at the top of the atmosphere, 0 at $p_* = 1/2$, to the value +1/2 at $p_* = 1$. Replacing s by -s in (3.5) it is seen that (3.5) goes into (3.4). The profiles (3.1) and (3.2) are therefore symmetric around $p_* = 1/2$, and they have the same values of I_1 and I_2 which implies that the complex phase speed is the same for the two profiles. In particular, we have shown that the rate of instability is the same for wind profiles which are symmetric around the middle of the atmosphere. The result would apparently not be true if the stratification was different from the adiabatic structure in the present model. The profiles shown in Figure 1 show several examples of such symmetric profiles such as (r,n), = (2,5) and (r,n) = (3,5), (r,n) = (2,6) and (r,n) = (4,6), (r,n) = (2,7) and (r,n) = (5,7) and several others.

The nondimensional phase speed, $c_* = c/U_m$, for the profile (3.1) can be evaluated from (2.3). We find that $I_1/U_m = 1$ and, after a simple integration,

$$F(r,n) = \frac{I_2}{U_m^2} = \left\{ \frac{(n-1)!}{(r-1)!(n-r-1)!} \right\}^2 \frac{(2r-2)!(2n-2r-2)!}{(2n-3)!} \tag{3.6}$$

The result is

$$c_* = \left(1 - \frac{\beta}{U_m} \frac{L^2}{8\pi^2}\right) \pm \left(1 - F(r,n) + \frac{\beta^2}{U_m^2} \frac{L^4}{64\pi^4}\right)^{1/2} \tag{3.7}$$

When the quantity under the square root is negative, we have instability. In this case we find

$$c_{*r} = 1 - \frac{\beta}{U_m} \frac{L^2}{8\pi^2} \tag{3.8}$$

and

$$c_{*i} = \left(F(r,n) - 1 - \frac{\beta^2}{U_m^2} \frac{L^4}{64\pi^4}\right)^{1/2} \tag{3.9}$$

which shows that the speed of the unstable waves are independent of the parameters r and n, but dependent on the vertically averaged speed U_m. (3.8) gives the well-known result that the speed of unstable waves in the present model is very similar to the speed of Rossby waves in a barotropic, nondivergent atmosphere.

(3.9) shows that sufficiently short waves are always unstable. The critical wavelength below which the waves are unstable is

$$L_c = 2\sqrt{2}\,\pi\left(\frac{U_m}{\beta}\right)^{1/2}\left(F(r,n) - 1\right)^{1/4} \tag{3.10}$$

which may also be written in the form

$$U_m = \frac{\beta}{8\pi^2}\,\frac{1}{c_{*i}(0)}\,L_c^2 \tag{3.11}$$

where

$$c_{*i}(0) = \left(F(r,n) - 1\right)^{1/2} \tag{3.12}$$

is the imaginary part of the phase speed at L = 0. It is seen from (3.11) that the region of instability is inside a parabola in a diagram with L as the abscissa and U_m as the ordinate. The region of instability is large if the coefficient to L_c^2 is small. The largest region of instability will be obtained for the maximum value of $c_{*i}(0)$.

Because of the fact that the instability is the same for two profiles which are symmetric around $p_* = 1/2$ we need consider only those profiles for which the maximum occurs at a nondimensional pressure $p_* \leq 1/2$. It is found by differentiation of (3.1) that

$$\frac{dU_N}{dp_*} = \frac{(n-1)!}{(r-1)!(n-r-1)!}\left\{(r-1) - (n-2)p_*\right\} p_*^{\,r-2}(1-p_*)^{n-r-2} \tag{3.13}$$

which shows that U_N has its maximum at a value of p_* equal to

$$p_{*,m} = \frac{r-1}{n-2} \tag{3.14}$$

We find $p_{*,m} \leq 1/2$ when $r \leq (1/2)n$ in agreement with the examples shown in Figure 1. It is of course common practice to illustrate the region of instability in a diagram with the windshear as ordinate and the wavelength as abscissa. We may define a windshear U_s by the formula

$$U_s = \frac{U_m}{1 - p_{*,m}} \int_{p_{*,m}}^{1} \left(-\frac{dU_N}{dp_*}\right) dp_* = \frac{U_m}{1 - p_{*,m}}\,U_N\left(p_{*,m}\right) \tag{3.15}$$

Using (3.14) and the definition of U_N we find

$$\frac{U_s}{U_m} = \frac{(n-1)!}{(r-1)!(n-r-1)!} \frac{(r-1)^{r-1}(n-r-1)^{n-r-2}}{(n-2)^{n-3}} \tag{3.16}$$

and (3.11) becomes

$$U_s = \gamma(r,n) L_c^2 \tag{3.17}$$

where

$$\gamma(r,n) = \frac{(n-1)!}{(r-1)!(n-r-1)!} \frac{(r-1)^{r-1}(n-r-1)^{n-r-2}}{(n-2)^{n-3}} \cdot \frac{\beta}{8\pi^2} \frac{1}{c_{*i}(0)} \tag{3.18}$$

A calculation of $\gamma(r,n)$ for various values of (r,n) shows the general result that the region of instability in a (L,U_s) plane becomes larger the closer the wind maximum is to any one of the boundaries $p_* = 0$ and $p_* = 1$. For a given value of r we find therefore the smallest region of instability when $n = 2r$, i.e., for the wind profile which is symmetric around $p_* = 1/2$. On the other hand, among these symmetric profiles we find the largest region of instability when $n = 2r$ is the largest, i.e., when we have the sharpest maximum. This result is in agreement with those obtained in the previous investigation.

In order to illustrate the degree of instability we have prepared Figure 2 which shows the e-folding time as a function of wavelength for the selections $(r,n) = (2,4), (2,5)\ldots,(2,8)$. These curves show that the degree of instability increases as the maximum of the wind profile approaches the upper boundary. Similar curves are naturally obtained if we let the wind maximum approach the lower boundary.

Figure 3 illustrates the degree of instability, measured by the e-folding time as a function of wavelength, for the wind profiles which are symmetric around $p_* = 1/2$. It is seen that the degree of instability increases as $n = 2r$ increases, i.e., the sharper the wind maximum becomes.

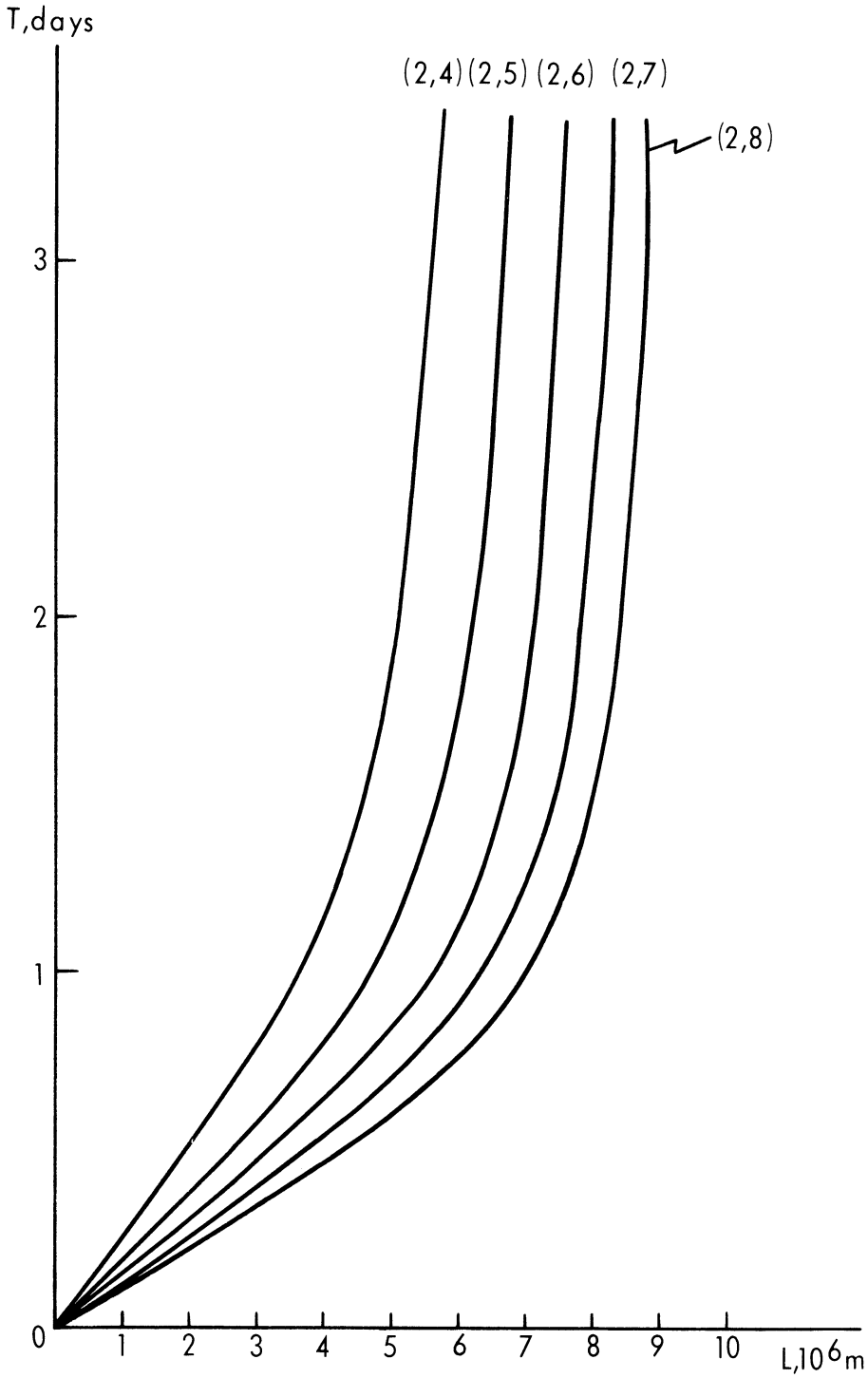

Figure 2. The e-folding time in days as a function of the wavelength in 10^6m for the values (r,n) = (2,4),(2,5),...,(2,8).

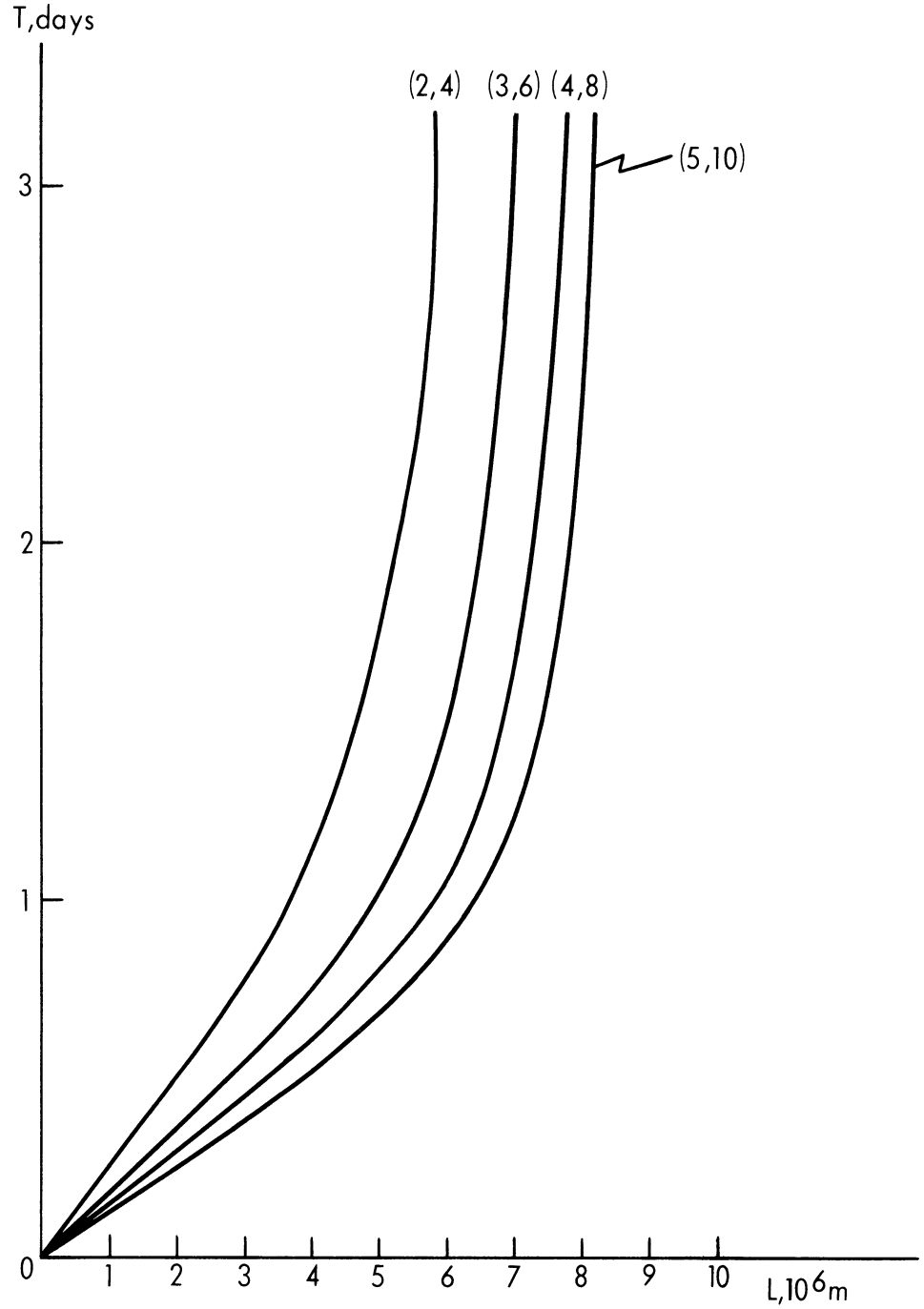

Figure 3. As Figure 2, but for the values (r,n) = (2,4), (3,6), (4,8), and (5,10).

4. Concluding Remarks

The purpose of this note has been to investigate the region and the degree of instability as a function of the vertical profile of the horizontal wind. In the quasi-geostrophic model with adiabatic stratification it is found that

(a) the instability is the same for two wind profiles which are symmetric around the middle of the atmosphere. A low level jet will thus show the same instability as a high level jet;

(b) the instability becomes larger the closer the jet is to either of the boundaries; and

(c) among the symmetric wind profiles those with the sharpest maximum will be the most unstable.

Reference

Wiin-Nielsen, A., 1967: On baroclinic instability as a function of the vertical profile of the zonal wind, Monthly Weather Review, Vol. 95, pp. 733-739.

A NOTE ON FJØRTOFT'S BLOCKING THEOREM

by

A. Wiin-Nielsen
Department of Atmospheric and Oceanic Science
The University of Michigan

Abstract

The changes of kinetic energy and enstrophy in a three-component system in a barotropic, nondivergent fluid are analysed in detail. For a given change of kinetic energy or enstrophy on the intermediate scale, the changes on the large and the small scale components are calculated. The conditions under which the change on the large-scale component is larger than the change on the small-scale component are found for both enstrophy and kinetic energy as a function of the latitudinal scale parameter.

1. Introduction

Fjørtoft's (1953) theorem states that kinetic energy must be transferred toward both larger and smaller scales in a two-dimensional, nondivergent flow. This property is due to the conservation of both kinetic energy and enstrophy in a barotropic flow. The theorem is most easily proven for a low-order system consisting of three components only. For such a system one can easily calculate the changes in the kinetic energy of the largest and the smallest scales for a given change of kinetic energy on the middle scale as it was done by Fjørtoft (loc. cit.).

In atmospheric flow we have on the average a maximum conversion of available potential energy to kinetic energy on a scale around longitudinal wave number 5-8. If Fjørtoft's theorem is applicable to the baroclinic atmospheric flow, one should expect a nonlinear transfer of kinetic energy from this scale to both larger and smaller scales. Data studies, summarized by Steinberg et al. (1971), show that such transfers can be computed from atmospheric data with a result in agreement with the theorem.

It has on occasion been stated that Fjørtoft's theorem implies a larger transfer of kinetic energy to the large scale than to the small scale. This implication is perhaps due to a printing mistake in the original paper on the subject or to an erroneous use of a mechanical analogy suggested by Charney (1966). It appears that observational studies (Steinberg et al. (1971), Saltzman (1970), Saltzman and Teweles (1964)) verify the statement, but it must be kept in mind that these observational studies are arranged according to the longitudinal wave numbers, while the theory is developed for spherical harmonics, and that rather arbitrary divisions in three wave groups have been used in these studies.

In view of the facts mentioned above it seems desirable to investigate the conditions under which a larger transfer of kinetic energy goes to the larger scales than to the smaller scales. The question can be answered by elementary calculations as long as we restrict ourselves to a three-component system. Such an analysis is given in the following section combined with a similar analysis for enstrophy changes.

2. Three-Component System

Let us assume that we consider an interactive three-component system. By this we mean that the longitudinal wave numbers m satisfy the selection rule as given by Platzman (1960), and that the meridional scale parameters $n_1 < n_2 < n_3$ satisfy the selection rule

$$n_3 - n_1 < n_2 < n_1 + n_3 \tag{2.1}$$

or, equivalently,

$$n_2 - n_1 < n_2 < n_3 < n_1 + n_3 \tag{2.2}$$

Denoting $q = n(n+1)$ we may express the conservation of energy and enstrophy by the relations

$$\Delta K_1 + \Delta K_2 + \Delta K_3 = 0$$

$$q_1 \Delta K_1 + q_2 \Delta K_2 + q_3 \Delta K_3 = 0 \tag{2.3}$$

Assuming a change ΔK_2 of kinetic energy on the intermediate scale we may find ΔK_1 and ΔK_3 from (2.3) giving

$$\Delta K_1 = -\frac{q_3 - q_2}{q_3 - q_1} \Delta K_2$$

$$\Delta K_3 = -\frac{q_2 - q_1}{q_3 - q_1} \Delta K_2 \tag{2.4}$$

Since each of the fractions in (2.4) is positive because $q_1 < q_2 < q_3$ we find that ΔK_1 and ΔK_3 have the same sign, opposite to the sign of ΔK_2. It is easy to show that

$$0 < \frac{q_3 - q_2}{q_3 - q_1} < 1$$

and

$$0 < \frac{q_2 - q_1}{q_3 - q_2} < 1 \tag{2.5}$$

showing that $|\Delta K_1| < |\Delta K_2|$ and $|\Delta K_3| < |\Delta K_2|$. We shall next investigate the conditions under which $\Delta K_1 / \Delta K_3$ is larger than 1. We find from (2.4) that

$$\frac{\Delta K_1}{\Delta K_3} = \frac{q_3 - q_2}{q_2 - q_1} \tag{2.6}$$

and it follows therefore that

$$\frac{\Delta K_1}{\Delta K_3} > 1 \tag{2.7}$$

if and only if

$$q_2 < (1/2)(q_1 + q_3) = q_A \tag{2.8}$$

where q_A is the arithmetric mean value of q_1 and q_3.

We may also express (2.3) in terms of the enstrophy for the components. We have then

$$\begin{aligned} \Delta E_1 + \Delta E_3 &= -\Delta E_2 \\ \frac{1}{q_1}\Delta E_1 + \frac{1}{q_3}\Delta E_3 &= -\frac{1}{q_2}\Delta E_2 \end{aligned} \tag{2.9}$$

which may be solved giving

$$\begin{aligned} \Delta E_1 &= -\frac{q_1}{q_2}\cdot\frac{q_3 - q_2}{q_3 - q_1}\Delta E_2 \\ \Delta E_3 &= -\frac{q_3}{q_2}\cdot\frac{q_2 - q_1}{q_3 - q_1}\Delta E_2 \end{aligned} \tag{2.10}$$

(2.10) may naturally be obtained directly from (2.4) by using the relationship $\Delta E = qa^{-2}\Delta K$ where a is the radius of the earth. (2.10) shows that ΔE_1 and ΔE_3 have the same sign, opposite to the sign of ΔE_2. We should now like to consider the conditions under which $\Delta E_1/\Delta E_3$ is larger than unity. We find that this is the case if and only if

$$q_2 < \frac{q_1 q_3}{(1/2)(q_1 + q_3)} = \frac{q_G^2}{q_A} \tag{2.11}$$

where q_G, the geometrical mean, is defined by the relation $q_G = (q_1 q_3)^{1/2}$.

It is well-known that $q_A > q_G$. From this relation it follows that $q_A > q_G^2/q_A$. In view of this relation it is seen that if $\Delta E_1/\Delta E_3 > 1$, then it is also true that $\Delta K_1/\Delta K_3 > 1$. Conversely, we may say that if $\Delta K_1/\Delta K_3 < 1$ it follows that $\Delta E_1/\Delta E_3 < 1$. The condition which corresponds to the results of observational studies, i.e., $\Delta K_1/\Delta K_3 > 1$ and $\Delta E_1/\Delta E_3 < 1$, will take place in a three-component system only when $q_G^2/q_A < q_2 < q_A$.

These selection rules can easily be used to test any three-component system which has been selected for integration. If the system shall be active by which we mean that the interaction coefficient has a non-zero value we must also according to Platzman (1960) have

$$n_3 - n_1 < n_2 < n_3 \tag{2.12}$$

Suppose that we want to find the active systems for which $\Delta E_1/\Delta E_3 > 1$. Denoting $q_* = q_G^2/q_A$ we require

$$q_2 < q_*, \qquad n_2^2 + n_2 - q_* < 0 \tag{2.13}$$

which is satisfied if

$$n_2 < n_* = (1/4 + q_*)^{1/2} - 1/2 \tag{2.14}$$

In addition, we must satisfy (2.12). It is straightforward to show that $n_* < n_3$ in all cases. The final condition for $\Delta E_1/\Delta E_3 > 1$ is therefore

$$n_3 - n_1 < n_2 < n_* \tag{2.15}$$

(2.15) gives the lower and upper limit for n_2 necessary to insure that more enstrophy goes to the larger scale than to the smaller scale. These limits are easily calculated for a given pair (n_1, n_3). It is, however also seen from (2.15) that in order to find suitable values of n_2, it is a necessary condition that

$$n_3 - n_1 < n_* \tag{2.16}$$

(2.16) shows that the choice of (n_1,n_3) is restricted to a certain region in the first quadrant of the (n_1,n_3) plane. We shall next determine this region. Substituting from (2.14) in (2.16) and using the definitions of q_*, q_A and q_G we may after considerable algebraic manipulations show that (2.16) is equivalent to the following inequality:

$$F(n_1,n_3) < 0 \tag{2.17}$$

where

$$F(n_1,n_3) = n_1^2(n_1+1)(n_1-2n_3-1) - n_3(n_3+1)^2(2n_1-n_3) \tag{2.18}$$

To determine the region in which (2.17) is satisfied it is most convenient to find the roots of $F(n_1,n_3) = 0$ in the region $n_3 > n_1$. This was done by writing $F(n_1,n_3)$ as a 4th degree polynomial in n_3, determine the roots of the polynomial for a fixed value of n_1, and repeat the process by selecting a sufficient number of values of n_1. The results of these calculations are shown in Figure 1 in which the area between the curves $n_1 = n_3$ and $F(n_1,n_3)$ is the region in which $F(n_1,n_3) < 0$. For any pair of values of n_1 and n_3 selected within the region we can calculate the lower limit, i.e., $n_3 - n_1$, and the upper limit, i.e., n_*, for n_2 necessary to obtain $\Delta E_1/\Delta E_3 > 1$. It should be kept in mind that n_2 has to be an integer. $n_3 - n_1$ and n_* may be so close to each other that no integer can be found between them. Table I shows all the triplets (n_1,n_2,n_3) for which $\Delta E_1/\Delta E_3 > 1$. For each entry (n_1,n_3) for which $1 \le n_1 \le 17$ and $1 \le n_3 \le 20$ we have listed the permissible values of n_2 for which $\Delta E_1/\Delta E_3 > 1$.

Let us next turn our attention to the kinetic energy and find the triplets (n_1,n_2,n_3) for which $\Delta K_1/\Delta K_3 > 1$. We know that all the triplets listed in Table I will be included because it was shown earlier that if $\Delta E_1/\Delta E_3 > 1$ it follows that $\Delta K_1/\Delta K_3 > 1$, but it is likely that additional triplets will be included in the sample for which $\Delta K_1/\Delta K_3 > 1$. (2.7) and (2.8) show that the condition is fulfilled if

$$q < q_A, \qquad n_2^2 + n_2 - q_A < 0 \tag{2.19}$$

which is satisfied provided

$$n_2 < n_{**} = (1/4 + q_A)^{1/2} - 1/2 \tag{2.20}$$

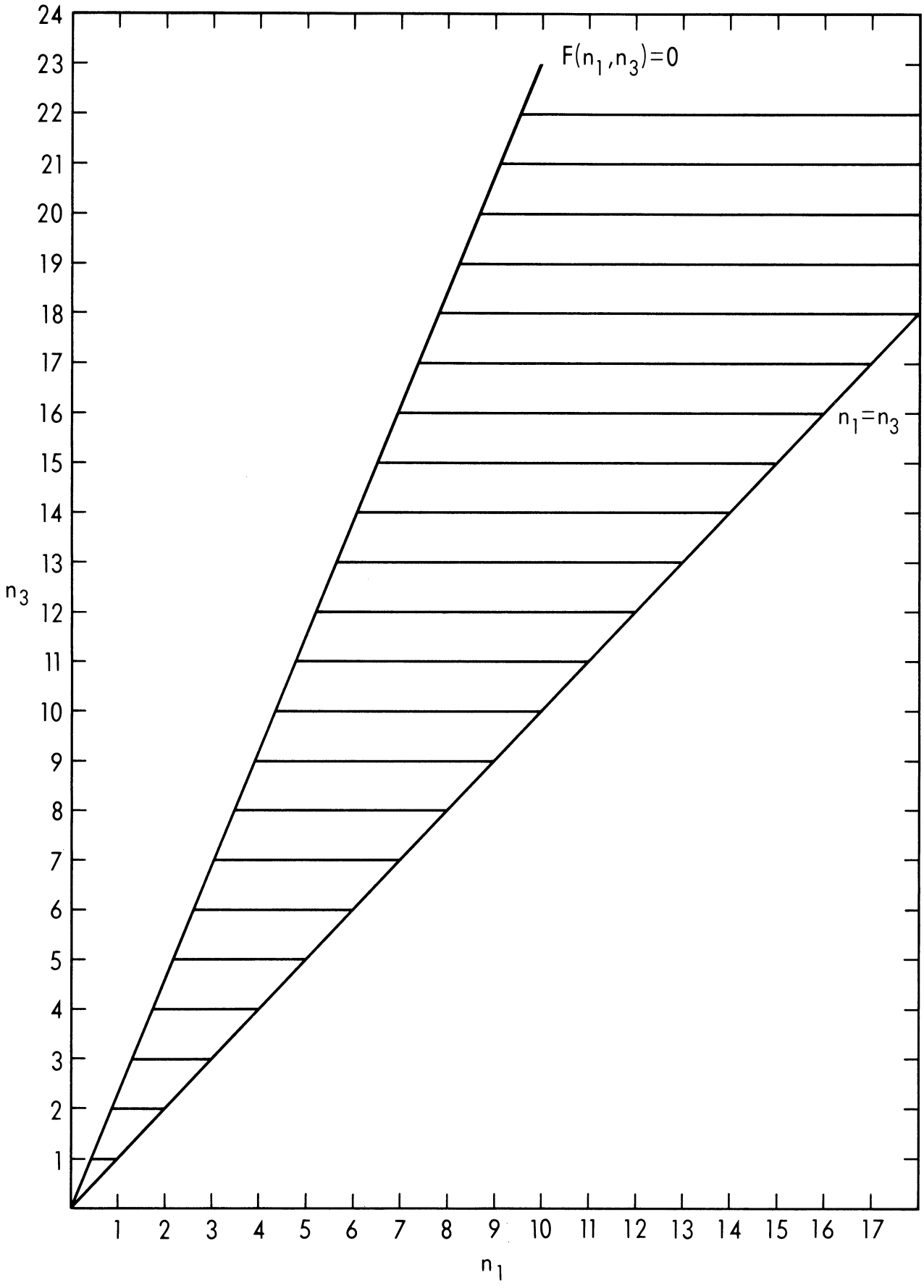

Figure 1. The necessary condition for the position (n_1,n_3) is between the curves $n_1 = n_3$ and $F(n_1,n_3) = 0$ in order to provide a possibility for satisfying the condition $\Delta E_1/\Delta E_3 > 1$.

TABLE I

VALUES OF n_2, FOR GIVEN VALUES OF n_1 AND n_3, FOR WHICH $\Delta E_1/\Delta E_3 > 1$

n_1 \ n_3	8	9	10	11	12	13	14	15	16	17	18	19	20
4	5												
5	6	6	6										
6		7	7	7	7								
7			8	8	8	8	8	9					
8				9	9	9	9	9,10	9,10	10			
9					10	10	10	10	10,11	10,11	10,11	11	
10						11	11	11	11,12	11,12	11,12	11,12	11,12
11							12	12	12	12,13	12,13	12,13	12,13
12								13	13	13	13,14	13,14	13,14
13									14	14	14	14,15	14,15
14										15	15	15	15,16
15											16	16	16
16												17	17
17													18

As before we must satisfy the selection rule

$$n_3 - n_1 < n_2 < n_3 \tag{2.21}$$

but it is straightforward to show that $n_{**} < n_3$ which indicates that $\Delta K_1/\Delta K_3 > 1$ if and only if

$$n_3 - n_1 < n_2 < n_{**} \tag{2.22}$$

The necessary condition restricting the choice of (n_1, n_3) is found, as in the previous case, by the inequality

$$n_3 - n_1 < n_{**} \tag{2.23}$$

leading to

$$G(n_1, n_3) = n_3^2 - (4n_1 - 1)n_3 + (n_1^2 - 3n_1) < 0 \tag{2.24}$$

which is straightforward to solve. Figure 2 shows the region in which $G(n_1,n_3) < 0$. We find as expected that this region is somewhat larger than the region in which $F(n_1,n_3) < 0$, see (2.17). As in the previous case we calculate from (2.22), with the definition of n_{**} in (2.20), the lower and upper limits of n_2 for each pair (n_1,n_3) satisfying $G(n_1,n_3) < 0$. The results are given in Table II where the entry of a single number indicates that n_2 can have this value only. On the other hand, an entry of a pair indicates that n_2 can take all values between the smaller and the larger number. For example, it is seen from Table II that if $n_1 = 9$ and $n_3 = 18$, n_2 may take the values 10, 11, 12, 13, 14 all of which will results in $\Delta K_1/\Delta K_3 > 1$.

In order to summarize the present investigation we have prepared Figure 3. The circles show those triplets for which $\Delta K_1/\Delta K_3 > 1$. For each pair (n_1,n_3) we have listed the minimum and maximum values of n_2 below the circle. Those circles for which $\Delta E_1/\Delta E_3 > 1$ have been filled, and the corresponding values of n_2 are given above the circle. The open circles indicate the triplets for which $\Delta K_1/\Delta K_3 > 1$ and $\Delta E_1/\Delta E_3 < 1$. In the sample given on Figure 3, i.e., $1 \leq n_1 \leq 18$, $1 \leq n_3 \leq 20$, there are 229 triplets for which $\Delta K_1/\Delta K_3 > 1$, but only 86 with $\Delta K_1/\Delta K_3 > 1$ and $\Delta E_1/\Delta E_3 > 1$, giving 143 cases with $\Delta K_1/\Delta K_3 > 1$ and $\Delta E_1/\Delta E_3 < 1$. It is thus seen that the latter category contains the majority of the cases.

3. Concluding Remarks

The main purpose of the present note has been to analyse a simple three-component system in a barotropic, non-divergent fluid with respect to energy and enstrophy transfers. Using the reasonable restriction that we consider active systems only we have found general conditions which determine the ratios of energy and enstrophy transfers to the large and the small scale for a given change on the intermediate scale. It cannot be concluded that there is always more energy transferred to the large scale and more enstrophy going to the small scale, but the investigations provide the formulas necessary to determine the ratios for any given three-component system.

4. Acknowledgments

The research has been supported by the National Science Foundation under Grant No. GA-16166. Mr. James Pfaendtner programmed the calculations leading to the determination of the criteria.

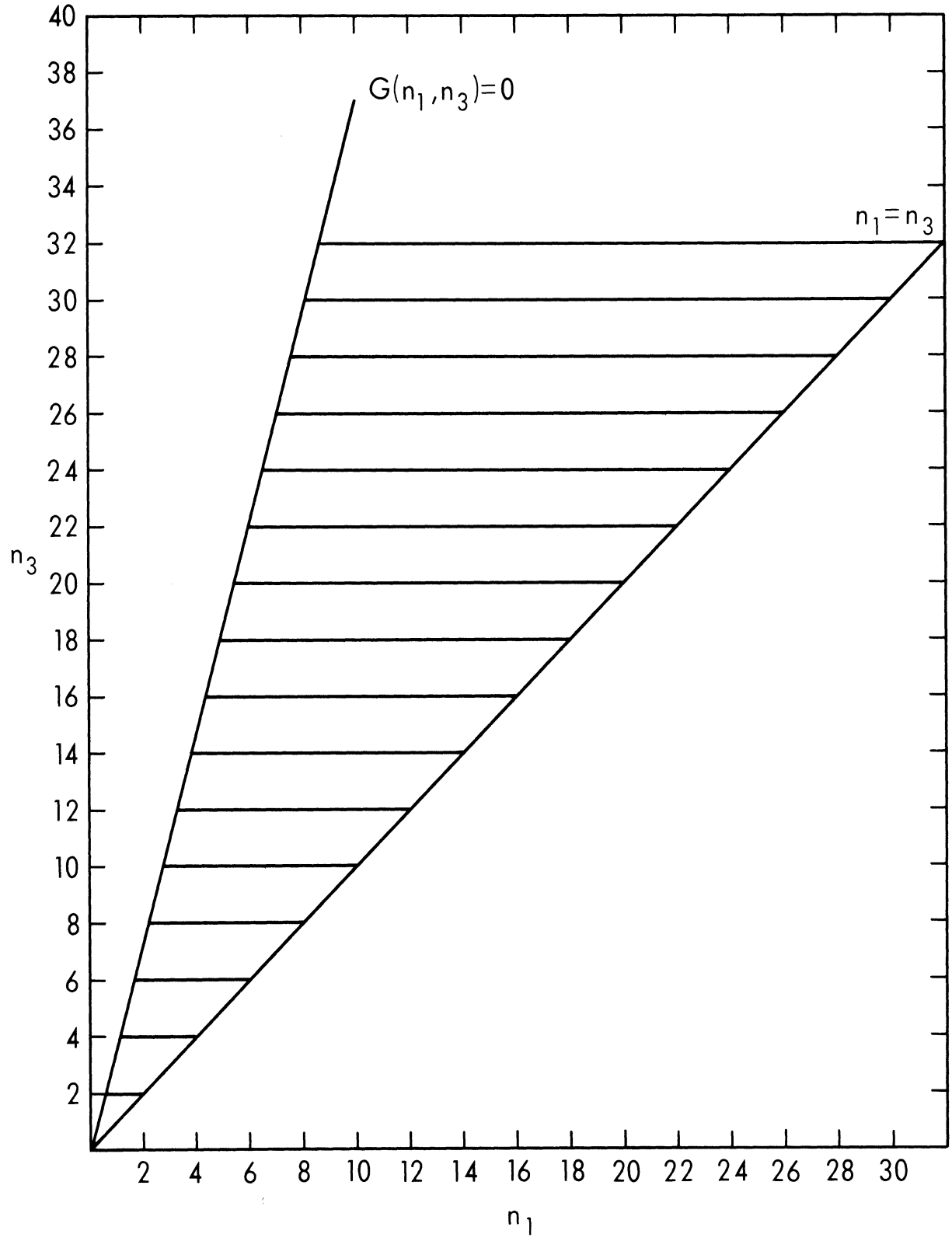

Figure 2. The region between the curves $n_1 = n_3$ and $G(n_1,n_3) = 0$ gives the positions of the point (n_1,n_3) necessary, but not sufficient, to satisfy the condition $\Delta K_1/\Delta K_3 > 1$.

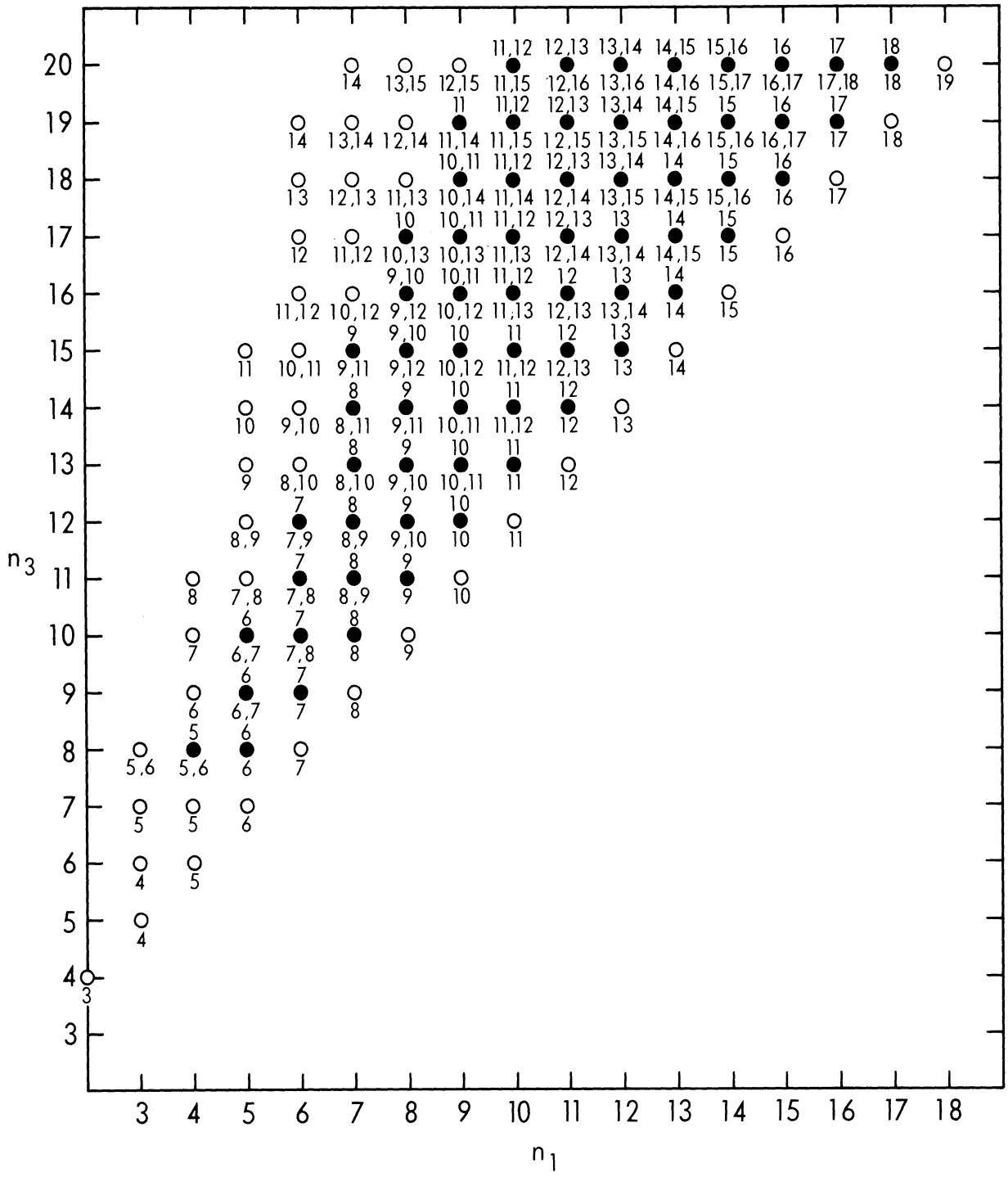

Figure 3. The circles indicate the points (n_1,n_3) for which $\Delta K_1/\Delta K_3 > 1$, if n_2 has any one of the values listed below the circle. The dots indicate the points (n_1,n_3) for which $\Delta K_1/\Delta K_3 > 1$ and $\Delta E_1/\Delta E_3 > 1$ if n_2 attains any of the values common to the sets listed above and below the dot.

TABLE II

VALUES OF n_2 FOR GIVEN VALUES OF n_1 AND n_3 FOR WHICH $\Delta K_1/\Delta K_3 > 1$

n_1 \ n_3	4	5	6	7	8	9	10	11	12	13	14	15	16	17	18	19	20
1																	
2	3																
3		4	4	5	(5,6)												
4			5	5	(5,6)	6	7	8									
5				6	6	(6,7)	(6,7)	(7,8)	(8,9)	9	10	11					
6					7	7	(7,8)	(7,8)	(7,9)	(8,10)	(9,10)	(10,11)	(11,12)	12	13	14	
7						8	8	(8,9)	(8,9)	(8,10)	(8,11)	(9,11)	(10,12)	(11,12)	(12,13)	(13,14)	14
8							9	9	(9,10)	(9,10)	(9,11)	(9,12)	(9,12)	(10,13)	(11,13)	(12,14)	(13,15)
9								10	10	(10,11)	(10,11)	(10,12)	(10,12)	(10,13)	(10,14)	(11,14)	(12,15)
10									11	11	(11,12)	(11,12)	(11,13)	(11,13)	(11,14)	(11,15)	(11,15)
11										12	12	(12,13)	(12,13)	(12,14)	(12,14)	(12,15)	(12,16)
12											13	13	(13,14)	(13,14)	(13,15)	(13,15)	(13,16)
13												14	14	(14,15)	(14,15)	(14,16)	(14,16)
14													15	15	(15,16)	(15,16)	(15,17)
15														16	16	(16,17)	(16,17)
16															17	17	(17,18)
17																18	18
18																	19
19																	

References

Charney, J. G., 1966: Some remaining problems in numerical weather prediction, Advances in Numerical Weather Prediction, Traveler's Research Center, Hartford, Connecticut.

Fjørtoft, R., 1953: On the changes in the spectral distribution of kinetic energy for two-dimensional, nondivergent flow, Tellus, Vol. 5, pp. 225-230.

Platzman, G. W., 1960: The spectral form of the vorticity equation, J. Meteor., Vol. 17, pp. 635-644.

Saltzman, B., 1970: Large-scale atmospheric energetics in the wave number domain, Reviews of Geophysics and Space Physics, Vol. 8, pp. 289-302.

Saltzman, B. and S. Teweles, 1964: Further statistics on the exchange of kinetic energy between harmonic components of the atmospheric flow, Tellus, Vol. 16, pp. 432-435.

Steinberg, H. L., A. Wiin-Nielsen and C.-H. Yang, 1971: On nonlinear cascades in large-scale atmospheric flow, J. Geophys. Res., Vol. 76, pp. 8629-8640.

Wiin-Nielsen, A., 1972: A study of power laws in the atmospheric kinetic energy spectrum using spherical harmonic functions, Meteorologiske Annaler, Vol. 6, No. 5, pp. 107-124.

A NOTE ON THE ANGULAR MOMENTUM BALANCE OF THE ATMOSPHERE

by

A. Wiin-Nielsen
Department of Atmospheric and Oceanic Science
The University of Michigan

Abstract

The vertically averaged meridional transport of momentum of the atmosphere is calculated under steady state conditions from a simple parameterization of the surface stress. The primary purpose of the calculation is to demonstrate that the major features of the momentum transport as derived from atmospheric data can be reproduced by the simple model.

1. Introduction

The qualitative aspects of the required meridional momentum transport of the atmosphere can easily be derived by a consideration of the surface stress which reduces the westerly momentum in the regions of surface westerlies and increase the westerly momentum (decrease the easterly momentum) in the region of surface easterlies. In order to maintain the momentum balance in a zonal ring extending from the surface of the earth to the top of the atmosphere it is necessary to transport westerly momentum from the the regions of surface easterlies to the regions of surface westerlies as first suggested by Jeffreys (1926) and later used by many authors. The fact that the surface stress may be calculated by a vertical integration of the equations of motion or, alternately, from the vorticity equation has been used to obtain information on the geographical distribution of the stress from upper wind information.

Adopting a relation between the surface zonal stress and the surface zonal wind as is generally done in models of the large-scale atmospheric circulation it is equally possible to calculate the vertically averaged, meridional transport of momentum. It is thus possible to ask if it is possible to reproduce the momentum transport as derived from atmospheric winds from the observed distribution of the surface zonal winds. The calculation of the zonal stresses from calculated momentum transports has been carried out by several authors (see, for example, Wiin-Nielsen et al. (1964)).

In the following sections we shall give a particularly simple example which may be used for educational purposes because it can be solved in a straightforward manner by analytical methods, but the general method may also be used to compute the meridional transport of momentum from a representative meridional profile of the zonally averaged wind.

2. Formulation of the Problem

It is well-known that the zonally averaged form of the first equation of motion may be written in the form

$$\frac{\partial u_z}{\partial t} + \frac{1}{a \cos^2\varphi} \frac{\partial (uv)_z \cos^2\varphi}{\partial \varphi} + \frac{\partial (u\omega)_z}{\partial p} = f v_z + F_{\lambda,z} \qquad (2.1)$$

in which u, v, and ω are the three components of the three-dimensional velocity vector, a is the radius of the earth, φ is latitude, p is pressure, and $F_{\lambda,z}$ is the zonal average of the zonal component of the frictional force per unit

mass. The subscript z denotes a zonal average, defined by the relation

$$( )_z = \frac{1}{2\pi} \int_0^{2\pi} ( ) \, d\lambda \tag{2.2}$$

The zonally averaged form of the continuity equation is

$$\frac{1}{a \cos\varphi} \frac{\partial v_z \cos\varphi}{\partial \varphi} + \frac{\partial \omega_z}{\partial p} = 0 \tag{2.3}$$

Adopting the boundary conditions $\omega_z = 0$ at $p = 0$ and $p = p_o = 100$ cb where the last condition is the common approximation and introducing a vertical average by the definition

$$( )_M = \frac{1}{p_o} \int_0^{p_o} ( ) \, dp \tag{2.4}$$

it follows from (2.3) that

$$v_{z,M} = 0 \tag{2.5}$$

Using (2.5) and the boundary conditions stated above it follows by applying (2.4) to (2.1) that

$$\frac{\partial u_{z,M}}{\partial t} + \frac{1}{a \cos^2\varphi} \frac{\partial (uv)_{z,M} \cos^2\varphi}{\partial \varphi} = F_{\lambda,z,M} \tag{2.6}$$

We shall now adopt the following expression for F_λ

$$F_\lambda = - g \frac{\partial \tau_\lambda}{\partial p} \tag{2.7}$$

where g is the acceleration of gravity and τ_λ the zonal component of the stress. It follows then from (2.4) that

$$F_{\lambda,z,M} = - \frac{g}{p_o} \tau_{\lambda,z,o} \tag{2.8}$$

where the subscript o denotes the value at $p = p_o$. We shall now further adopt the parameterization, common in large-scale models that

$$\tau_{\lambda,z,o} = \rho_o c_d V_o u_{zo} \tag{2.9}$$

where ρ_o is the density, c_d the surface drag coefficient, and V_o the windspeed at $p = p_o$. Introducing finally a steady state assumption in (2.6) we get

$$\frac{1}{a \cos^2\varphi} \frac{\partial M \cos^2\varphi}{\partial \varphi} = - \frac{g}{p_o} \rho_o c_d V_o u_{zo} \tag{2.10}$$

where we have introduced the notation $M = (uv)_{z,M}$. It is (2.10) which normally is the basis for a qualitative discussion of the requirements for the momentum transports in the atmosphere. (2.10) says that there must, under steady state conditions, be a convergence of the momentum transport when $u_z > 0$ and a divergence when $u_z < 0$. If we can get a numerical estimate of the coefficient to u_{zo} in (2.10), and if u_{zo} is specified in some fashion we may use (2.10) to calculate M by integration of (2.10).

3. A Simple Example

It is generally recognized that c_d and V_o are variables to which we have to assign typical values. We shall be using a normalized form of M when computed, and it is therefore of no great concern which numerical values we assign. Let us denote

$$\varepsilon = \frac{g}{p_o} \rho_o c_d V_o = \frac{g c_d V_o}{R T_o} \tag{3.1}$$

Using $g = 9.8$ m sec^{-2}, $c_d = 3 \times 10^{-3}$, $V_o = 10$ m sec^{-1}, $R = 287$ m^2 sec^{-2} deg^{-1}, and $T_o = 288°K$, we find $\varepsilon = 3.56 \times 10^{-6}$ sec^{-1}.

The meridional distribution of u_{zo}, applicable to steady state conditions, is characterized by easterlies in the low latitudes, westerlies in the middle latitudes, and weak easterlies in the high latitudes. A simple expression which behaves in this fashion is

$$u_{zo} = - U_o \cos 4\varphi \tag{3.2}$$

We shall now calculate M from (2.10) using (3.2) for u_{zo}. We obtain

$$M \cos^2\varphi = - \varepsilon a U_o \int_{\varphi}^{\pi/2} \cos(4\varphi) \cos^2\varphi \, d\varphi \tag{3.3}$$

which upon integration gives

$$M = A \sin(2\varphi)\,(3-4\sin^2\varphi) \tag{3.4}$$

where

$$A = (1/6)\varepsilon a U_o = 18.9\ m^2\ sec^{-2} \tag{3.5}$$

adopting $U_o = 5\ m\ sec^{-1}$.

Figure 1 shows M calculated from (3.4) and normalized in such a way that the maximum value is unity (left side). The same figure shows u_{zo} (right side) normalized in the same way. A comparison between Figure 1 and similar figures based upon observed winds prepared by Starr et al. (1970), shows that the simple example depicts the major features of the "observed" distribution of M although it should be noted that the figures given by Starr et al. (loc. cit.), shows M $\cos^2\varphi$. This difference accounts for the much smaller values shown in the negative transports in the very high latitudes in the study based on observations.

We shall next calculate M from a representative profile of $u_z(\varphi)$. For this purpose we have calculated the profile from the climatological data for the Southern Hemisphere given by Van Loon et al., (1971). The annual average of u_{zo}, computed as the mean of the data given for the four months: January, April, July, and October, is shown in Figure 2. M was computed by a numerical integration of (2.10). The values of M, normalized in such a way that the minimum value is -1, are shown in Figure 3 as the solid curve. The agreement between the momentum transport from our simple example shown in Figure 1 and Figure 3 is obvious indicating that our example is quite representative.

The circles entered on Figure 3 is the total momentum transport for the Southern Hemisphere calculated on the basis of Obasi's (1963) investigation which used IGY data for the calendar year 1958. The general shape of M from these data is the same, but the northward transport in the high latitudes is considerably larger in 1958 than in the climatological average.

4. Concluding Remarks

The principle used in this note has been used several times to calculate the surface stress from upper wind statistics. We have emphasized that a parameterization of the surface stress in terms of the surface winds permits a

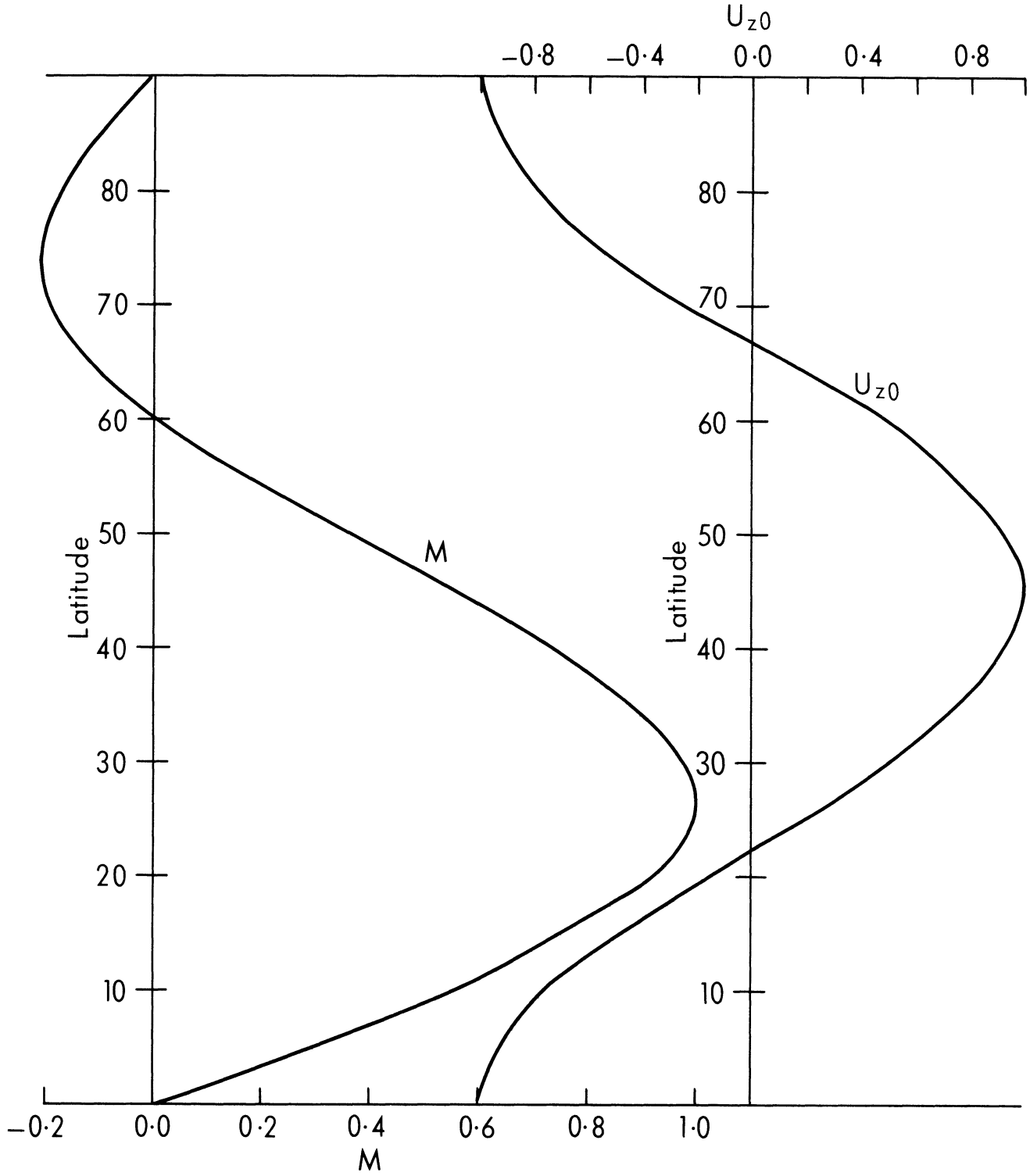

Figure 1. The right part shows the specified zonally averaged wind at the surface (upper scale) as a function of latitude, while the left part shows the meridional momentum transport, both normalized with respect to their maximum value (lower scale).

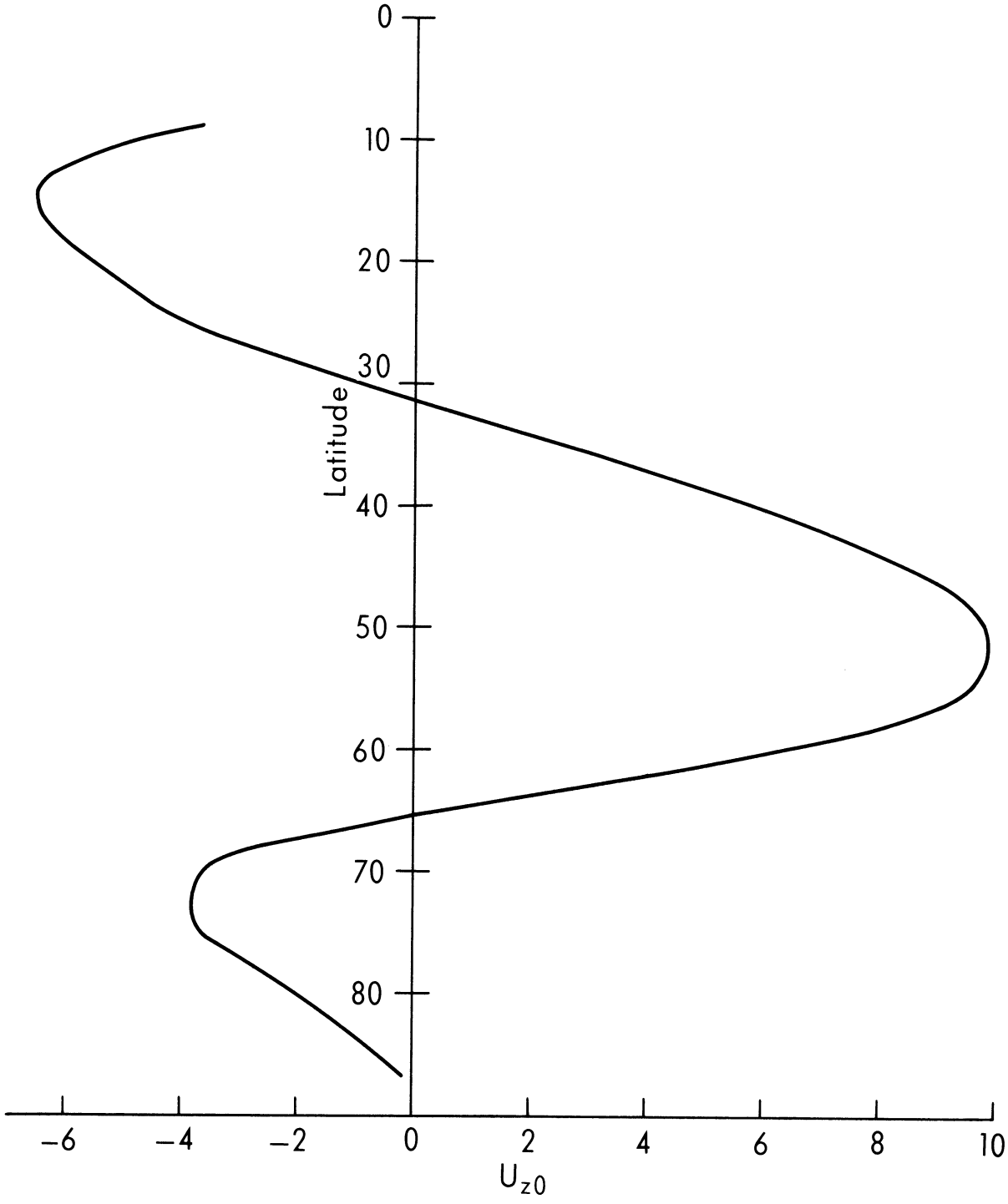

Figure 2. The zonally averaged surface geostrophic wind in m sec^{-1} as a function of latitude. The curve is the annual average for the Southern Hemisphere.

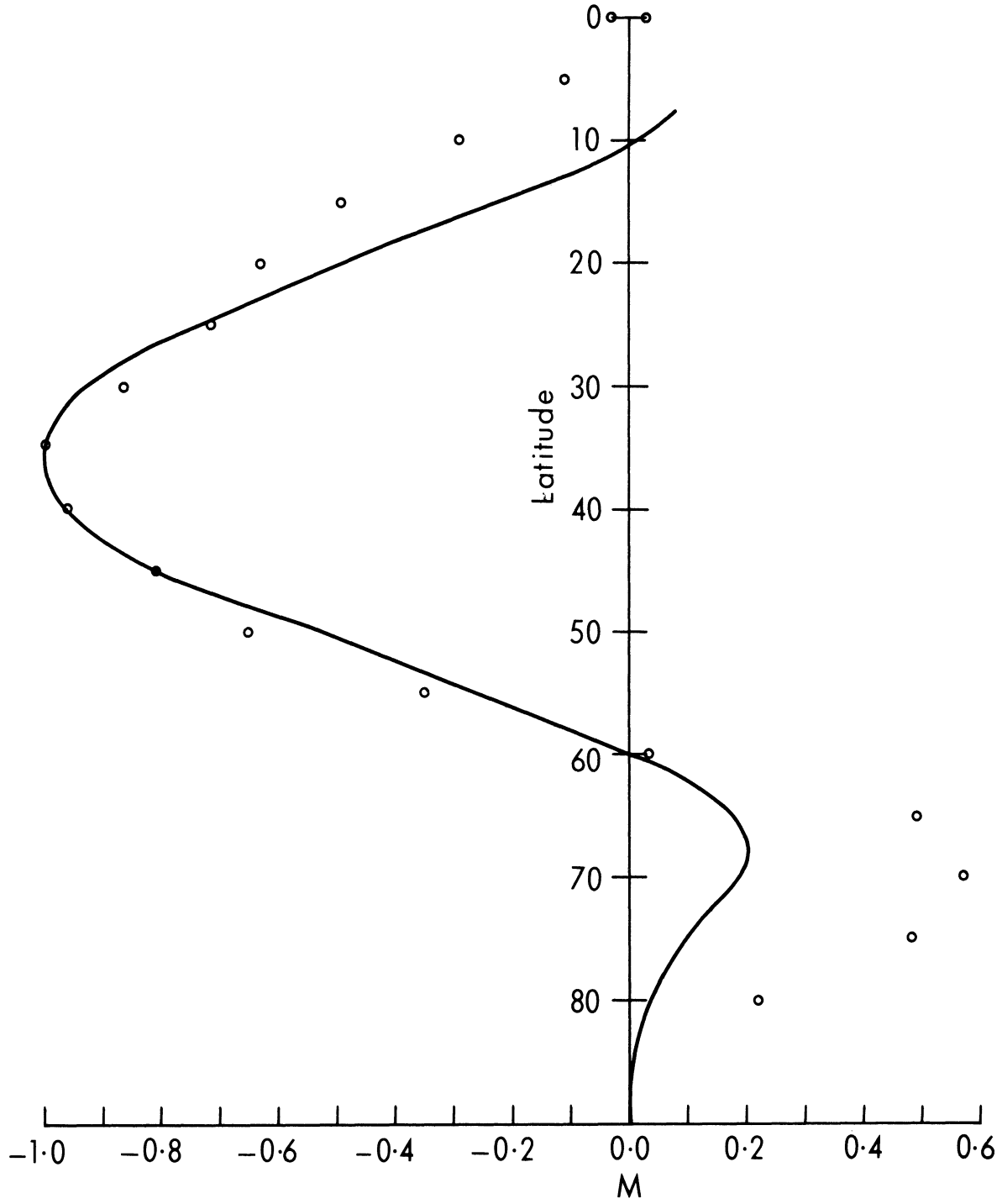

Figure 3. The meridional, vertically averaged momentum transport computed from the data given in Figure 2. Circles are obtained from Obasi (1963).

calculation of the total meridional transport of momentum. Such calculations, using a simple analytical example and statisitics of the surface wind, have been carried out with fair agreement with other direct calculations of the vertically averaged, meridional momentum transport.

References

Jeffreys, H., 1926: On the dynamics of the geostrophic winds, Quart. J. Roy. Meteorol. Soc., Vol. 152, pp. 85-104.

Obasi, G.O.P., 1963: Poleward flux of atmospheric angular momentum in the southern hemisphere, J. Atmos. Sci., Vol. 20, pp. 516-528.

Starr, V. P., J. P. Peixoto, and N. E. Gaut, 1970: Momentum and zonal kinetic energy balance of the atmosphere from five years of hemispheric data, Tellus, Vol. 22, pp. 251-274.

Van Loon H., J. J. Taljaard, R. L. Jenne, and H. L. Cratcher, 1971: Climate of the upper air: southern hemisphere, Vol. II, zonal geostrophic winds National Center for Atmospheric Research, NCAR TN/STR-57.

Wiin-Nielsen, A., J. A. Brown, and M. Drake, 1964: Further studies of energy exchange between the zonal flow and the eddies, Tellus, Vol. 15, pp. 261-279.